Hybrid method of generating spin-squeezed states for quantum-enhanced atom interferometry

Liam A. Fuderer, Joseph J. Hope ⬤, and Simon A. Haine

Department of Quantum Science and Technology, Research School of Physics, The Australian National University, Canberra 0200, Australia

We introduce a spin-squeezing technique that is a hybrid of two well-established spin-squeezing techniques, quantum nondemolition measurement (QND), and one-axis twisting (OAT). This hybrid method aims to improve spin-squeezing over what is currently achievable using QND and OAT. In practical situations, the strength of both the QND and OAT interactions is limited. We find that, in these situations, the hybrid scheme performed considerably better than either OAT or QND used in isolation. As QND and OAT have both been realized experimentally, this technique could be implemented in current atom interferometry setups with only minor modifications to the experiment.

I. INTRODUCTION

Atom interferometry is capable of providing state-of-the-art measurements of gravitational fields [1–7], gravitational gradients [8–13], and magnetic fields [14], with future applications such as minerals exploration [15,16], hydrology [17], inertial navigation [18–20], and possible tests of candidate theories of quantum gravity [21–23]. There is considerable recent interest in the use of quantum entanglement in atom interferometry [24–26], which would improve the precision, measurement rate, and reduce the overall size of these devices [25]. Two of the most promising routes to generating useful entanglement are spin squeezing via one-axis twisting (OAT) [27–30], or via quantum nondeomolition (QND) measurements [31–37]. These methods have been used in proof of principle experiments [38,39], but have not yet found utility in a state-of-the-art inertial sensors. In particular, typical atom interferometry experiments with ultra-cold atoms have only modest optical densities, and permit only modest levels of squeezing via QND [40]. While the use of an optical cavity can significantly improve the amount of achievable squeezing [35,36,38,39], this adds considerable experimental overhead, increasing the size, weight, and complexity of the experiment [19].

A recent proposal showed that, in a freely expanding Bose-Einstein condensate (BEC), strong atom-atom interactions can generate substantial spin squeezing via OAT between two momentum modes without degrading mode overlap or causing significant phase diffusion, and could potentially allow for a high precision, spin-squeezed gravimetry measurement [41]. However, only a modest level of OAT interactions are achievable via this method, as the interactions are quickly reduced due to the expansion of the atomic clouds. Here, we present a hybrid scheme that utilizes both QND and OAT. In particular, by combining both schemes, we can achieve levels of squeezing significantly higher than either scheme on their own. When restricting ourselves to the small levels of QND interaction that free-space QND permits and the weak OAT interaction that would be generated via the scheme presented in Szigeti *et al.* [41], we show that combining these schemes

can give significantly better levels of squeezing than either in isolation. Furthermore, these schemes are entirely compatible and can be implemented together without compromising the performance of either one.

II. COMBINING QND AND OAT TO IMPROVE SPIN SQUEEZING

We will begin by describing the hybrid scheme and then going into the details of each element, specifically, the QND and OAT interactions. Assuming a BEC of N atoms with two hyperfine states $|1\rangle$ and $|2\rangle$, we introduce the pseudospin operators $\hat{J}_k = \frac{1}{2}(\hat{a}_1^\dagger \, \hat{a}_2^\dagger)\sigma_k(\hat{a}_1 \, \hat{a}_2)^T$, where σ_k is the kth Pauli matrix and $\hat{a}_1$ and $\hat{a}_2$ are the annihilation operators for atomic states $|1\rangle$ and $|2\rangle$, respectively. These two states may also carry an associated momentum difference, such as is the case in an atom interferometer used to measure gravity. When used as the input to a Mach-Zehnder interferometer, the achievable phase-sensitivity is

$$\Delta\phi = \frac{\xi}{\sqrt{N}}, \tag{1}$$

where

$$\xi = \sqrt{N}\frac{\sqrt{\text{Var}(\hat{J}_z)}}{|\langle\hat{J}_x\rangle|}, \tag{2}$$

where ξ is the Wineland spin-squeezing parameter [42], with $\xi < 1$ indicating spin squeezing. The hybrid scheme involves first applying the QND interaction and then using the OAT interaction to further enhance the squeezing (see Fig. 1). Specifically, we initially prepare our system with all atoms in state $|1\rangle$ (maximum $\hat{J}_z$ eigenstate), before applying a beam-splitter pulse which puts each atom in an equal coherent superposition of $|1\rangle$ and $|2\rangle$. This is a rotation about the $\hat{J}_y$ axis by $\pi/2$, creating a coherent spin-state (CSS) on the equator of the Bloch sphere, or a maximal $\hat{J}_x$ eigenstate. The QND interaction reduces the uncertainty in the $\hat{J}_z$ axis, while increasing fluctuations in the $\hat{J}_y$ axis. The state is then rotated by an angle θ_{QND} about the $\hat{J}_x$ axis, before the OAT interaction is applied, which causes a nonlinear "shearing"
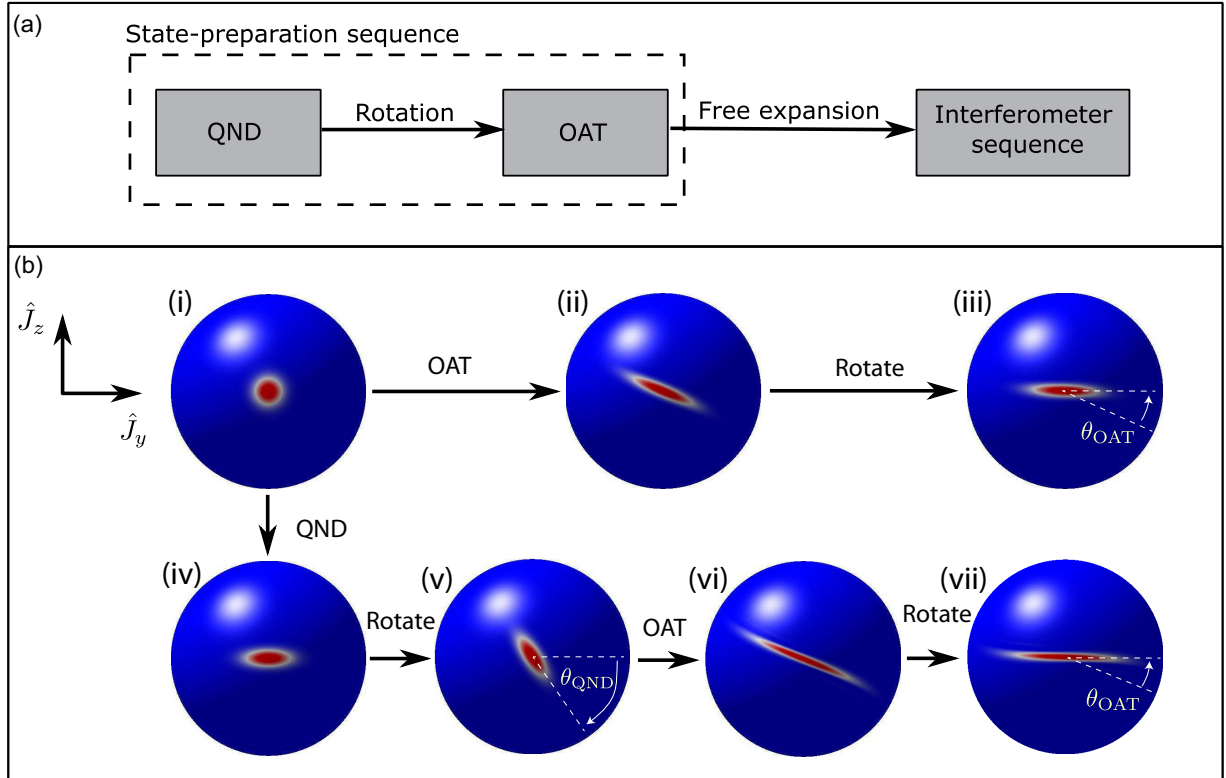
FIG. 1. (a) Hybrid method schematic. The model is a modification to the current OAT state-preparation sequence. The output state from the hybrid model is used as the initial state for the interferometer sequence. (b) Bloch sphere representation of OAT (top row) and the proposed hybrid method (bottom row) for an initial CSS. In OAT, the initial CSS (i) undergoes nonlinear shearing creating a state with reduced variance in some direction (ii). This state is then rotated about the J_x axis by an amount θ_{OAT} to create a state with reduced variance in the J_z axis (iii). In the hybrid method, the initial state first undergoes QND squeezing, creating a state with reduced variance in the J_z axis (iv). This state is then rotated about the J_x axis by an amount θ_{QND} (v), such that it undergoes more rapid shearing under OAT dynamics (vi). This state is then rotated by amount θ_{OAT} to reduce the variance in the J_z direction. When the degree of OAT or QND interaction is limited, the hybrid scheme can produce better spin squeezing than either OAT or QND used in isolation.

of the state. Rotating the QND state before the OAT interaction increases the variance in $\hat{J}_z$, which causes the state to shear faster under the OAT interaction, ultimately increasing the amount of spin squeezing achievable. The value of θ_{QND} that optimizes the spin-squeezing parameter depends on both the amount of QND interaction before, and OAT interaction after the rotation. The QND interaction is achieved via an optical coupling, and can occur on timescales much faster than the atomic dynamics, while the OAT interaction is achieved via utilization of the interatomic interactions, and typically takes several milliseconds to achieve significant shearing. As these two interactions utilize different resources, they are entirely compatible and can be applied sequentially as described above. As QND and OAT have both been realized experimentally, this technique could be implemented in current atom interferometry setups with only minor modifications to the experiment. Specifically, as described in [41], OAT can be achieved by replacing the free-expansion time with two additional beamsplitter pulses, implemented via the same laser system as the interferometric pulses. QND is achieved by using an off-resonant laser (or a pair of lasers, one for each hyperfine state) to perform state-dependent number estimation of the sample after an initial additional beamsplitter pulse.

We will describe the dynamics of this scheme quantitatively in Sec. III. We will now briefly review the principles and

performance of the OAT and QND interactions individually, before assessing the performance of the hybrid scheme.

A. QND Squeezing

By illuminating the atomic sample with a laser detuned from some excited state $|e\rangle$, the population in each of the hyperfine states $|a_1\rangle$ and $|a_2\rangle$ is imprinted on the phase of the light. Consequently, a measurement of the phase allows one to infer information about the population difference, collapsing the atomic state into a spin-squeezed state (SSS), with reduced variance in $\hat{J}_z$ [24,43]. As the collapse is random, feedback (via a rotation around the $\hat{J}_y$ axis of magnitude proportional to the measurement result) is used to recenter the state on the equator, such that $\langle \hat{J}_z \rangle = 0$. The amount of spin squeezing depends on the strength of the atom-light entanglement. QND can be achieved using monochromatic (one-color) [44], or dichromatic (two-color) laser light [40,45]. One-color QND is susceptible to dephasing of the atoms due to the inhomogeneous spatial profile of the laser, which degrades spin squeezing [46]. Two-color QND rectifies this issue and suppresses experimental noise, such as vibrations in mirror positions, to first order. Assuming the laser is spatially homogeneous, both methods can be shown to have the same spin squeezing. For simplicity, we will therefore proceed with a
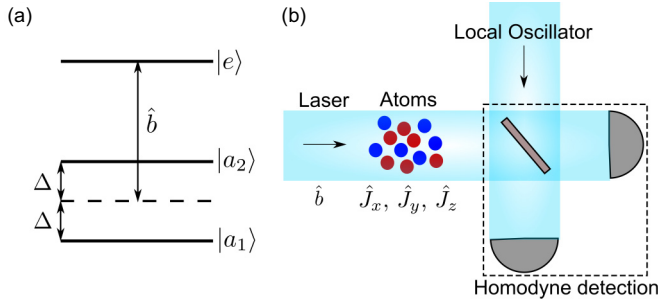
FIG. 2. (a) Energy-level diagram of quantum nondemolition measurements. The atoms are illuminated by a laser (annihilation operator $\hat{b}$) equally detuned from the two atomic levels, $|a_1\rangle$ and $|a_2\rangle$, to an excited state $|e\rangle$. This imprints the difference in the number of atoms in each state $\hat{J}_z$ into the phase of the laser. (b) Schematic of experimental quantum nondemolition measurement in free space. After the laser passes through the atoms, the phase is measured by a homodyne detector, allowing for an inference of $\hat{J}_z$ to be made. Such an inference reduces the variance in $\hat{J}_z$ and thus creates a SSS

one-color QND model without loss of generality, although a two-color scheme may be favorable for experimental implementation.

A schematic of the atom-light interaction is shown in Fig. 2. A single laser is detuned from resonance by an amount $(-)\Delta$ for the $|a_{1(2)}\rangle \rightarrow |e\rangle$ transition. Adiabatically eliminating the excited state [43] $|e\rangle$ gives the effective Hamiltonian

$$\hat{H}_{\text{QND}} = -\hbar\chi_{\text{QND}}\hat{J}_z\hat{b}^\dagger\hat{b}, \tag{3}$$

where $\hat{b}$ is the annihilation operator for a pulse of light of duration t_p and χ_{QND} is the atom-light interaction strength, which for the detuning Δ shown in Fig. 2 is

$$\chi_{\text{QND}} = \frac{2\sigma_0\Gamma}{A\Delta t_p}. \tag{4}$$

Here, σ_0 is the resonant scattering cross section, Γ is the transition spontaneous emission rate, and A is the cross-sectional area of the laser incident on the atomic sample.

The degree of spin squeezing is well characterized by the resonant optical depth d and the inelastic scattering rate integrated over the pulse duration η, which can be written in terms of the system parameters as

$$d = \frac{\sigma_0 N}{A}, \tag{5}$$

$$\text{and } \eta = \frac{2\sigma_0}{A}\left(\frac{\Gamma}{\Delta}\right)^2 N_p, \tag{6}$$

where N_p is the total photon number. Due to the narrow momentum linewidth of the Bose-Einstein condensate, any spontaneous emissions causes the atom to be scattered into a distinguishable momentum state, and is therefore lost from the interference measurement [40]. We treat these spontaneous emission events by coupling vacuum noise fluctuations into the atomic operators [47].

For a fixed resonant optical depth, there is a trade-off between the amount of information inferred about the population difference and information lost due to spontaneous emission, as seen in the inset of Fig. 3. Optimizing over the loss fraction
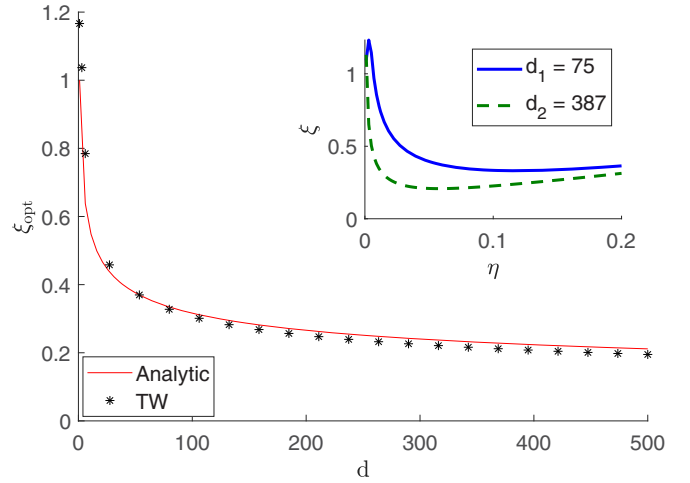

FIG. 3. Optimum spin-squeezing parameter ξ_{opt} from QND on the D1 line of a system of 10^5 ^{87}Rb atoms, calculated via truncated Wigner (black stars), compared to analytic scaling $\xi_{\text{opt}} = d^{-1/4}$ (red solid line). Inset figure: Scaling of the spin-squeezing parameter ξ with the loss fraction η for a fixed resonant optical depth. Outer figure: The optimal spin-squeezing parameter as a function of optical depth, found by minimization of ξ with respect to η, for $d = d_1 = 75$ (blue solid line) and $d = d_2 = 387$ (green dashed line). ξ_{opt} scales as $d^{-1/4}$.

gives [31,45,48] an optimum squeezing of

$$\xi_{\text{opt}} \approx d^{-1/4}. \tag{7}$$

For Bose-condensed atoms, the atomic density is limited by three-body recombination, which ultimately limits the achievable optical depth. For fixed atomic density, adjusting the aspect ratio of the BEC to a cigar-shaped cloud with the long-axis aligned with the tightly focused probe beam increases the optical density. In this geometry, the limiting factor now becomes the Rayleigh length of the beam. Confining the atoms to a cylinder of diameter equal to the beam waste and length equal to the Rayleigh length, and optimizing the size of the beam waist gives a maximum optical depth of

$$d \leqslant \sigma_0\sqrt{\frac{N\rho}{\lambda}}, \tag{8}$$

where ρ is the atomic density and λ is the optical wavelength. For a $N = 10^5$ ^{87}Rb BEC using the D1 line, optimizing the optical depth for a fixed atomic density of $10^{14}/\text{cm}^3$, gives an optical depth of $d = 387$, and $\xi_{\text{opt}} \approx 0.23$. To further improve the achievable squeezing, the effective optical depth, and therefore the achievable level of QND squeezing further, a high finesse optical cavity could be employed.

B. One-axis twisting

One-axis twisting (OAT) dynamics is caused by a Hamiltonian of the form

$$\hat{H}_{\text{OAT}} = \hbar\chi_{\text{OAT}}(t)\hat{J}_z^2, \tag{9}$$

and leads to correlations between the relative number difference and relative phase degrees of freedom [27]. This results in a "shearing" of the quantum state on the Bloch sphere, and
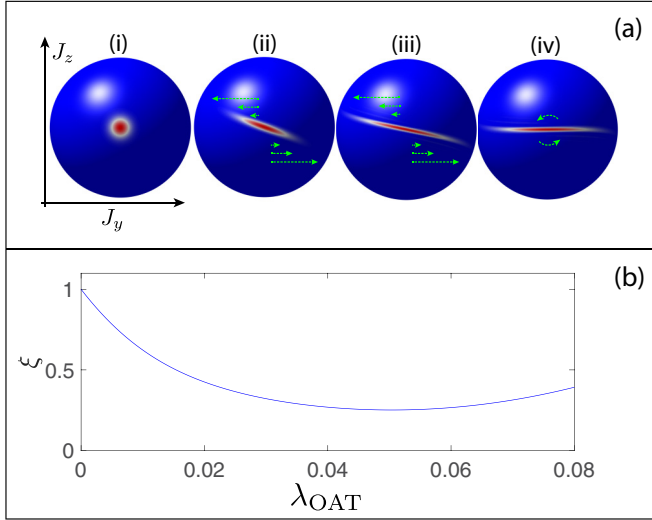
FIG. 4. (a) Evolution of the Wigner quasiprobability distribution for an initial coherent spin state of 100 atoms under OAT dynamics, for (i) $\lambda_{OAT} = 0$, (ii) $\lambda_{OAT} = 0.025$, (iii) $\lambda_{OAT} = 0.05$, (iv) $\lambda_{OAT} = 0.05$, with an additional rotation around the $\hat{J}_x$ axis applied to convert the squeezing into the $\hat{J}_z$ direction. (b) Spin-squeezing parameter as a function of λ_{OAT}.

a narrowing of the spin distribution along one axis (Fig. 4). In a two-component BEC, OAT dynamics naturally arises from the interatomic interactions [28,49–54]. Introducing the usual Bosonic field operators for hyperfine state $|j\rangle$, $\hat{\psi}_j(\mathbf{r})$, which obey the usual commutation relations

$$[\hat{\psi}_i(\mathbf{r}), \hat{\psi}_j^\dagger(\mathbf{r}')] = \delta_{ij}\delta(\mathbf{r} - \mathbf{r}'), \quad (10)$$

the Hamiltonian term describing interatomic interactions is

$$\hat{H}_{int} = \sum_{i,j} \frac{U_{ij}}{2} \int \hat{\psi}_i^\dagger(\mathbf{r})\hat{\psi}_j^\dagger(\mathbf{r})\hat{\psi}_i(\mathbf{r})\hat{\psi}_j(\mathbf{r}) \, d^3\mathbf{r}. \quad (11)$$

Making a single-mode approximation as in [53], $\hat{\psi}_i(\mathbf{r}, t) \approx \hat{a}_i u_i(\mathbf{r}, t)$ and ignoring terms linear in $\hat{J}_z$, we recover Eq. (9), with $\chi(t) = 4[\chi_{11}(t) + \chi_{22}(t) - 2\chi_{12}(t)]$, with

$$\chi_{ij}(t) = \frac{U_{ij}}{2\hbar} \int |u_i(\mathbf{r}, t)|^2 |u_j(\mathbf{r}, t)|^2 \, d^3\mathbf{r}. \quad (12)$$

The total effective OAT interaction is then given by the unitary $\hat{U}_{OAT} = \exp(-i\lambda_{OAT}\hat{J}_z^2)$, where $\lambda_{OAT} = \int_0^T \chi(t)dt$, and T is the duration of the state preparation time. In the recent proposal by Szigeti *et al.* [41], it was shown that spin squeezing could be created by inducing significant OAT dynamics by spatially separating the two clouds during the usual pre-expansion phase that usually proceeds atom interferometry. This sets $\chi_{12} \to 0$, significantly increasing χ. As the clouds then expand, the magnitude of χ decreases to zero, causing λ_{OAT} to plateau. Benchmark calculations place the maximum interaction strength currently achievable at $\lambda_1 = 6.5 \times 10^{-5}$ for a system of $N = 10^5$ atoms [41], which is considerably less than the optimum value for this number of atoms ($\lambda_{opt} \approx 53 \times 10^{-5}$). However, our recent calculations indicate that interaction strengths of up to $\lambda_2 = 9.8 \times 10^{-5}$ are possible by instantaneously applying an inwards focusing potential

immediately before expansion, in a similar method to that proposed by the authors of [55]. This value of λ_{OAT} is based on modeling the delta-kick scheme proposed by the authors of [55] using the same simulation technique as in [41]. These results are currently being prepared for publication. We use these values as references throughout our discussion.

III. SIMULATING THE HYBRID METHOD

To simulate the combination of QND and OAT dynamics, we cannot simply rely on simple models that give the spin-squeezing parameter for QND dynamics. This is because we need to know the form of the full quantum state to perform the subsequent OAT dynamics. In particular, the magnitude of the antisqueezing in the conjugate ($\hat{J}_y$) axis will have a significant effect on the subsequent OAT evolution. The truncated Wigner (TW) method [56] has been successfully used to simulate BEC dynamics [57–60]. Importantly, the TW method can be used to model the production of nonclassical correlations within the condensate [61–64] including those generated OAT [41,52,53,65] and atom-light interactions [40,66]. The TW method also works well for large numbers of atoms and can easily incorporate loss due to spontaneous emission. The derivation of the TW method has been described in detail elsewhere [57,67,68]. Briefly, the equation of motion for the Wigner function for the system can be found from the von Neumann equation by using correspondences between differential operators on the Wigner function and the original quantum operators [69]. By truncating third- and higher-order derivatives (the TW approximation), a Fokker-Planck equation (FPE) is obtained. The FPE is then mapped to a set of stochastic differential equations for complex variables $\{\alpha_1(t), \alpha_2(t), \beta(t)\}$, which loosely correspond to the annihilation operators of the system $\{\hat{a}_1(t), \hat{a}_2(t), \hat{b}(t)\}$, with initial conditions stochastically sampled from the appropriate Wigner distribution [68,70]. Moments of observables are then calculated via the mapping $\langle\{f(\hat{a}_1, \hat{a}_1^\dagger, \hat{a}_2, \hat{a}_2^\dagger, \hat{b}, \hat{b}^\dagger)\}_{sym}\rangle \to \overline{f(\alpha_1, \alpha_1^*, \alpha_2, \alpha_2^*, \beta, \beta^*)}$, where "sym" denotes symmetric ordering and the overline denotes the mean over many stochastic trajectories.

A. QND simulation

We begin by simulating the QND dynamics of a series of light pulses, each of duration t_p, interacting with the BEC sequentially. In the absence of loss due to spontaneous emission, mapping Eq. (3) to the TW method, we find

$$i\frac{d}{dt}\alpha_1 = \frac{\chi_{QND}}{2}|\beta_j|^2\alpha_1, \quad (13a)$$

$$i\frac{d}{dt}\alpha_2 = \frac{\chi_{QND}}{2}|\beta_j|^2\alpha_2, \quad (13b)$$

$$i\frac{d}{dt}\beta_j = \chi_{QND}\mathcal{J}_z\beta_j, \quad (13c)$$

where $\mathcal{J}_z = \frac{1}{2}(|\alpha_1|^2 - |\alpha_2|^2)$ and β_j is the TW variable associated with the jth pulse. By assuming our pulses are short compared to the relevant atomic timescales, we can take the

continuum limit by introducing the parameter

$$\beta(t) = \frac{1}{\sqrt{t_p}} \sum_j \Pi_j(t)\beta_j, \tag{14}$$

where

$$\Pi_j(t) = \begin{cases} 1 & \text{if } jt_p < t \leqslant (j+1)t_p, \\ 0 & \text{otherwise.} \end{cases} \tag{15}$$

By taking the limit $t_p \to 0$, these equations can be solved analytically to give

$$\alpha_1(t) = \exp\left(-i\frac{\lambda_{\text{QND}}}{2}N_p(t)\right)\alpha_1(0), \tag{16a}$$

$$\alpha_2(t) = \exp\left(i\frac{\lambda_{\text{QND}}}{2}N_p(t)\right)\alpha_2(0), \tag{16b}$$

$$\beta(t) = \exp\left(-i\lambda_{\text{QND}}\mathcal{J}_z\right)\beta(0), \tag{16c}$$

where $N_p(t) = \int_0^t |\beta(t')|^2 dt$,

$$\lambda_{\text{QND}} = \chi_{\text{QND}}t_p = \frac{2\sigma_0\Gamma}{A\Delta}, \tag{17}$$

and the initial condition are given by

$$\alpha_1(0) = \sqrt{\frac{N_t}{2}} + v_1, \tag{18a}$$

$$\alpha_2(0) = \sqrt{\frac{N_t}{2}} + v_2, \tag{18b}$$

$$\beta_{\text{in}}(t) = \beta_0 + w(t), \tag{18c}$$

where v_j is complex Gaussian noise satisfying $\overline{v_i^*v_j} = \frac{\delta_{ij}}{2}$, and $\overline{w^*(t)w(t')} = \frac{1}{2}\delta(t - t')$.

We introduce the effect of spontaneous emission by noting that the fraction of atoms lost from each component in the duration of one pulse is $f = 1 - e^{-\eta(t)}$, where

$$\eta(t) = \frac{2\sigma_0}{A}\left(\frac{\Gamma}{\Delta}\right)^2 |\beta_0|^2 t. \tag{19}$$

By treating loss from the atomic system as an introduction of vacuum noise in the standard way [40], we obtain

$$\alpha_1(t) = \exp\left(-i\frac{\lambda_{\text{QND}}}{2}N_p(t)\right)\alpha_1(0)\sqrt{1 - f(t)}$$
$$+ \sqrt{f(t)}v_1(0), \tag{20a}$$

$$\alpha_2(t) = \exp\left(i\frac{\lambda_{\text{QND}}}{2}N_p(t)\right)\alpha_2(0)\sqrt{1 - f(t)}$$
$$+ \sqrt{f(t)}v_2(0), \tag{20b}$$

$$\beta_{\text{out}}(t) = \exp[-i\lambda_{\text{QND}}\mathcal{J}_z(t)]\beta_{\text{in}}(t), \tag{20c}$$

where $v_j(0)$ is complex Gaussian noise satisfying $\overline{v_i^*v_j} = \frac{\delta_{ij}}{2}$. Here, we define $\beta_{\text{out}}(t)$ as the light exiting the BEC after interacting with the atoms, and $\beta_{\text{in}}(t)$ as the input light.

Equations (20) create correlations between the relative population imbalance of the atoms and the phase of the light. To convert this into spin squeezing, the population imbalance is inferred from the phase quadrature of the light, which is obtained via homodyne measurement, and is represented by

the quantity

$$Y = \frac{1}{\sqrt{T}} \int_0^T i[\beta_{\text{out}}(t) - \beta_{\text{out}}^*(t)]dt. \tag{21}$$

This information is then used to implement the feedback step by rotating the atomic state around the $\hat{J}_y$ axis by an angle θ_y proportional to the result of a measurement on the quadrature of the light. Specifically, we perform the transformation

$$\alpha_1 \to \cos\frac{\theta_y}{2}\alpha_1 + \sin\frac{\theta_y}{2}\alpha_2, \tag{22a}$$

$$\alpha_2 \to \cos\frac{\theta_y}{2}\alpha_2 - \sin\frac{\theta_y}{2}\alpha_1, \tag{22b}$$

where

$$\theta_y = \sin^{-1}\left(\frac{Y}{\lambda_{\text{QND}}N_t\beta_0 T}\right). \tag{23}$$

The spin-squeezing parameter calculated via this method is shown in Fig. 3 and shows excellent agreement with the analytic solution.

B. Combining OAT and QND

To simulate the hybrid scheme, we take the solution of equations [20], perform a rotation by an amount θ_{QND}, and use this as the initial condition for the OAT dynamics. OAT dynamics is simulated in TW via mapping Eq. (9) to the set of ODEs for the TW variables

$$i\frac{d}{dt}\alpha_1 = \frac{\chi(t)}{2}(|\alpha_1|^2 - |\alpha_2|^2)\alpha_1, \tag{24a}$$

$$i\frac{d}{dt}\alpha_2 = -\frac{\chi(t)}{2}(|\alpha_1|^2 - |\alpha_2|^2)\alpha_2, \tag{24b}$$

which has the simple analytic solution

$$\alpha_1(t) = \exp\left(-i\frac{\lambda_{\text{OAT}}(t)}{2}(|\alpha_1|^2 - |\alpha_2|^2)\right)\alpha_1(0), \tag{25a}$$

$$\alpha_2(t) = \exp\left(i\frac{\lambda_{\text{OAT}}(t)}{2}(|\alpha_1|^2 - |\alpha_2|^2)\right)\alpha_2(0). \tag{25b}$$

After these dynamics, the state is rotated around the J_x axis by an angle θ_{OAT} to minimize the variance in J_z.

To gain some intuition about the hybrid dynamics, we first simulate the system in the absence of spontaneous emission. Figure 5 shows how the spin-squeezing parameter evolves under OAT dynamics from an initially spin-squeezed state, compared to an initial CSS. Importantly, the role of the pre-OAT rotation by θ_{QND} is clearly illustrated: for angles that increase the initial value of $V(\hat{J}_z)$ to larger than a CSS, the OAT dynamics occurs much faster. When a smaller rotation angle is used, slightly better spin squeezing is achieved, at the expense of much slower evolution.

When loss is included in the QND model, the final state after the QND interaction is no longer a minimum uncertainty state. The extra antisqueezing in the J_y direction will negatively affect the efficacy of the subsequent OAT dynamics. Figure 6 shows the spin-squeezing parameter including loss in the QND calculation, optimized over η and θ_{QND}, compared to purely OAT dynamics, for realistic values of λ_{OAT}, i.e., $\lambda_{\text{OAT}} \leqslant 2 \times 10^{-4}$. We considered three optical depths
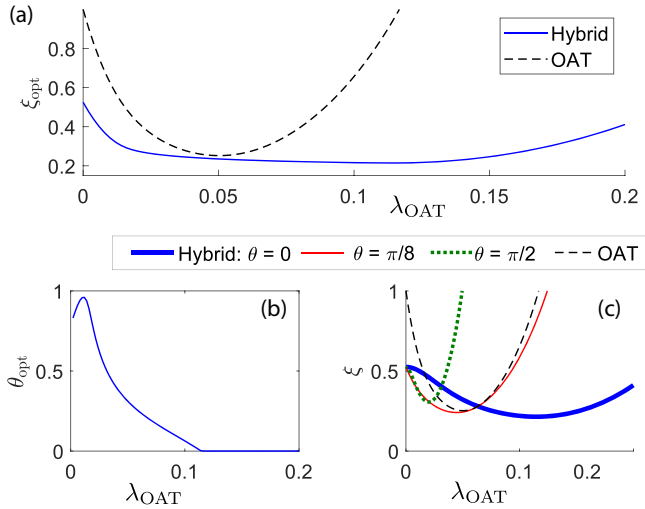
FIG. 5. Comparison of OAT and the hybrid scheme in the absence of loss from QND, for 100 atoms. After QND, the state has a spin-squeezing parameter of $\xi = 0.5$. (a) ξ versus λ_{OAT} for three different values of θ_{QND}. Large angles increase the rate of spin squeezing, but a worse optimum. (b) Optimal value of θ_{QND} as a function of λ_{OAT}. Once $\lambda_{OAT} \gg \lambda_{opt}$, the optimum angle reduces to zero to capitalize on the increased spin squeezing of states with small initial variance in J_z. (c) Spin-squeezing parameter optimized over θ_{QND}. The hybrid model outperforms OAT over all interaction strengths.
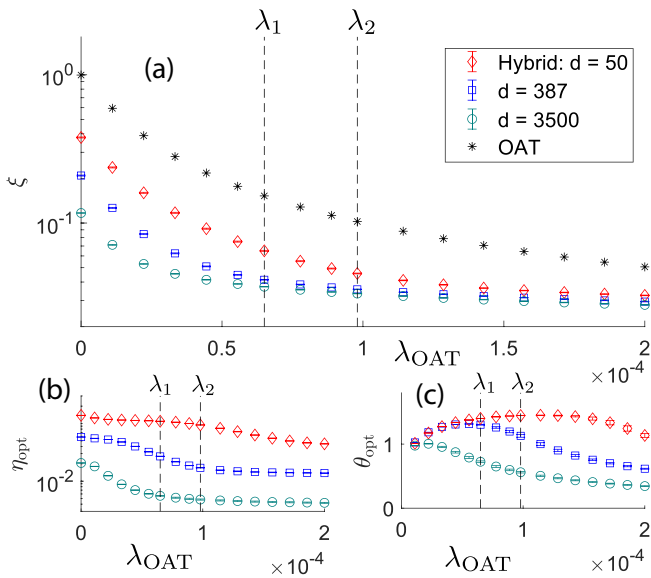

FIG. 6. (a) Squeezing parameter as a function of λ_{OAT} for the hybrid scheme compared to OAT, for three optical depths $d = 50$ (red), 387 (blue), and 3500 (green). The hybrid method is optimized over η and θ. The dashed lines represent the OAT interaction strengths achievable via the scheme presented in [41], ($\lambda_{OAT} = \lambda_1$), and using a delta-kick scheme ($\lambda_{OAT} = \lambda_2$). The hybrid method significantly outperforms the OAT scheme at both interaction strengths. (b) Optimal measurement strength η versus λ_{OAT}. η_{opt} decreases as λ_{OAT} increases as a consequence of OAT being more efficient for higher purity states. (c) Optimal rotation angle versus λ_{OAT}. The behavior of the rotation angle qualitatively mimics the lossless results.
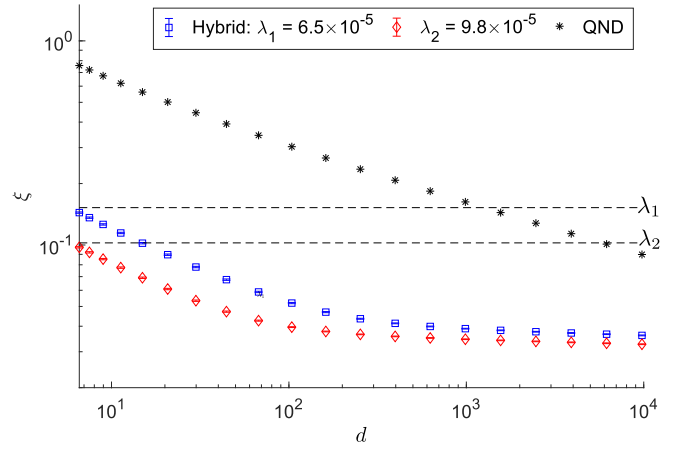

FIG. 7. Squeezing parameter scaling against resonant optical depth of the BEC for only QND (black), and the optimized hybrid method for a OAT interaction strength of λ_1 (blue) and λ_2 (red). Optical depths of $d > 387$ require a cavity. The dashed lines represent OAT spin squeezing at λ_1 and λ_2, respectively. QND at $d = 10^4$ represents the best spin squeezing available in experiments. The hybrid method exceeds this limit for $d > 10$ at both interaction strengths.

corresponding to different exemplary QND laser configurations: $d = 50$, a poorly focused laser in free space [$A = (1.5 \text{mm})^2$]; $d = 387$, an optimally focused laser in free space [$A = (0.53 \text{ mm})^2$]; and $d = 3500$, an optimally focused laser in a high-finesse optical cavity. with finesse $\mathcal{F} = 10^4$. The hybrid method outperformed OAT over all interaction strengths for each optical depth. For experimentally realizable interaction strengths $\lambda_{OAT} \leqslant \lambda_1$, the high-finesse cavity achieved the most spin squeezing by a significant margin. As the interaction strength increases, however, this advantage diminishes. Specifically, at λ_1, the amount of spin squeezing afforded by the optimal laser in free space was on par with the high-finesse cavity, being roughly four times the spin-squeezing of OAT performed in isolation. Furthermore, at λ_2, all three optical depths were comparable, providing roughly 2.5 times the spin squeezing of OAT.

Figure 7 shows the scaling of optimal QND spin squeezing against different optical depths. For both interaction strengths, the hybrid model significantly outperformed QND. Specifically, at $d = 387$, the hybrid method spin-squeezed five times (5.8 times) more than optimal QND for total interaction λ_1 (λ_2). These results are unsurprising, as we expect OAT to enhance spin-squeezing of a QND SSS. However, the hybrid method is also seen to outperform QND in an ultra-high-finesse cavity ($d = 10^4$), the current leader in spin-squeezing demonstrated in proof-of-principle experiments [38]. Specifically, the hybrid method outperformed in-cavity QND for optical depths of $d \approx 10$, meaning there is a large tolerance for imperfect laser focus. In addition, at the highest free-space optical depth, $d = 387$, the hybrid method provides 2.5 times the amount of spin squeezing over in-cavity QND. We therefore conclude that an experimental implementation of the hybrid method with modest requirements on size, weight, and power requirements could significantly increase spin-squeezing over QND.
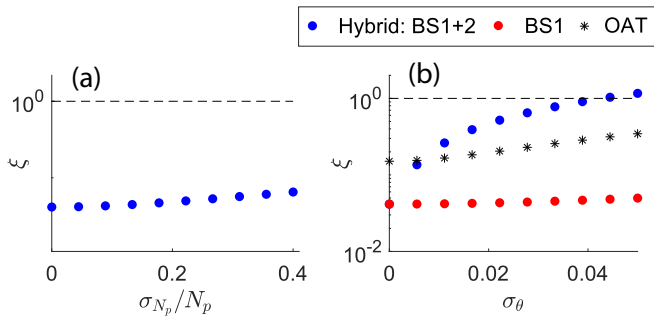
FIG. 8. (a) Squeezing parameter scaling against an introduced deviation in photon number (which controls the quantum nondemolition measurement strength) for the hybrid squeezing method. The parameter changes minimally for a deviation up to 30% of the photon number. (b) Squeezing parameter scaling against an introduced variance in rotation angle.

IV. EFFECT OF EXPERIMENTAL IMPERFECTIONS

While laser power may be stable over a single QND measurement, it may vary over multiple experiments. We incorporate these effects as fluctuations in the total photon during a QND measurement while fixing the beamsplitters before and after OAT is performed. Figure 8(a) shows how the optimized hybrid method is affected by these changes for OAT interaction $\lambda_1 = 6.5 \times 10^{-5}$. For fluctuations up to 30% of the total photon number, there is virtually no change in spin squeezing. Thus, the hybrid model is robust to fluctuations in the power of the laser used to perform QND.

We also investigate the effect of fluctuations in the power of the beamsplitter pulses. These will manifest as stochastic noise in the rotation angle of the state. Assuming only low-frequency noise, the angle will vary from shot-to-shot, rather than a single run, so we set the fluctuation in both beamsplitters to be the same. The impact on the optimized hybrid model for OAT interaction λ_1 is shown in Fig. 8(b). Fluctuations of 0.05 radians in both beamsplitters is shown to completely wash out the spin squeezing of the hybrid model (blue points). However, this is not an issue with the hybrid model, but rather of the stringent requirements for manipulating entangled states. Indeed, even for OAT performed on a CSS, much of the benefit is lost with fluctuations in the

second beamsplitter (black asterisks). Furthermore, the hybrid scheme is seen to be robust to fluctuations in only the first beamsplitter up to 0.05 radians (red dots), indicating that the second beamsplitter is responsible for the degradation in squeezing. The hybrid method therefore has more stringent stability requirements than OAT and QND, but only due to complications with manipulating entangled states.

V. CONCLUSION

Our investigation of a hybrid method of QND and OAT indicates that significant gains to precision can be made with current state-of-the-art experiments without imposing high size, weight, and power requirements. We demonstrated that, by first performing QND followed by OAT, the amount of spin squeezing that can be achieved is greater than both OAT and in-cavity QND. As both of the techniques were demonstrated in proof-of-principle experiments, the hybrid method can be incorporated with only small modifications to the experimental apparatus and procedure. Furthermore, we demonstrated that the hybrid method is robust to fluctuations in laser power when performing QND calculations, but is still subject to the stringent requirements of fluctuations in beamsplitter power for highly entangled states. The discussion in this paper has been limited to a single-mode model of OAT, which will need to be extended to a multimode model for more realistic predictions of spin squeezing.

This work has focussed on atomic interactions to achieve OAT dynamics. OAT dynamics can also be achieved by atom-light coupling via cavity feedback [35], and has been used to create spin-squeezing [36,71,72]. Interaction-based readouts [73] have also been performed via this method [74]. As it is possible to smoothly transition between cavity-based OAT and QND dynamics [75], exploration of the hybrid method in these systems is an exciting direction for future research.

[1] A. Peters, K. Y. Chung, and S. Chu, Measurement of gravitational acceleration by dropping atoms, Nature (London) **400**, 849 (1999).

[2] A. Peters, K. Y. Chung, and S. Chu, High-precision gravity measurements using atom interferometry, Metrologia **38**, 25 (2001).

[3] Z.-K. Hu, B.-L. Sun, X.-C. Duan, M.-K. Zhou, L.-L. Chen, S. Zhan, Q.-Z. Zhang, and J. Luo, Demonstration of an ultrahigh-sensitivity atom-interferometry absolute gravimeter, Phys. Rev. A **88**, 043610 (2013).

[4] M. Hauth, C. Freier, V. Schkolnik, A. Senger, M. Schmidt, and A. Peters, First gravity measurements using the mobile atom interferometer GAIN, Appl. Phys. B **113**, 49 (2013).

[5] V. Menoret, P. Vermeulen, N. Le Moigne, S. Bonvalot, P. Bouyer, A. Landragin, and B. Desruelle, Gravity measurements below 10^{-9} g with a transportable absolute quantum gravimeter, Sci. Rep. **8**, 12300 (2018).

[6] K. Bongs, M. Holynski, J. Vovrosh, P. Bouyer, G. Condon, E. Rasel, C. Schubert, W. P. Schleich, and A. Roura, Taking atom interferometric quantum sensors from the laboratory to real-world applications, Nat. Rev. Phys. **1**, 731 (2019).

[7] M. Kritsotakis, S. S. Szigeti, J. A. Dunningham, and S. A. Haine, Optimal matter-wave gravimetry, Phys. Rev. A **98**, 023629 (2018).

[8] M. J. Snadden, J. M. McGuirk, P. Bouyer, K. G. Haritos, and M. A. Kasevich, Measurement of the earth's gravity gradient

with an atom interferometer-based gravity gradiometer, Phys. Rev. Lett. **81**, 971 (1998).

[9] J. M. McGuirk, G. T. Foster, J. B. Fixler, M. J. Snadden, and M. A. Kasevich, Sensitive absolute-gravity gradiometry using atom interferometry, Phys. Rev. A **65**, 033608 (2002).

[10] F. Sorrentino, Q. Bodart, L. Cacciapuoti, Y.-H. Lien, M. Prevedelli, G. Rosi, L. Salvi, and G. M. Tino, Sensitivity limits of a Raman atom interferometer as a gravity gradiometer, Phys. Rev. A **89**, 023607 (2014).

[11] G. W. Biedermann, X. Wu, L. Deslauriers, S. Roy, C. Mahadeswaraswamy, and M. A. Kasevich, Testing gravity with cold-atom interferometers, Phys. Rev. A **91**, 033629 (2015).

[12] G. D'Amico, F. Borselli, L. Cacciapuoti, M. Prevedelli, G. Rosi, F. Sorrentino, and G. M. Tino, Bragg interferometer for gravity gradient measurements, Phys. Rev. A **93**, 063628 (2016).

[13] P. Asenbaum, C. Overstreet, T. Kovachy, D. D. Brown, J. M. Hogan, and M. A. Kasevich, Phase shift in an atom interferometer due to spacetime curvature across its wave function, Phys. Rev. Lett. **118**, 183602 (2017).

[14] M. Vengalattore, J. M. Higbie, S. R. Leslie, J. Guzman, L. E. Sadler, and D. M. Stamper-Kurn, High-resolution magnetometry with a spinor Bose-Einstein condensate, Phys. Rev. Lett. **98**, 200801 (2007).

[15] M. I. Evstifeev, The state of the art in the development of onboard gravity gradiometers, Gyroscopy Navig. **8**, 68 (2017).

[16] R. Geiger, A. Landragin, S. Merlet, and F. P. D. Santos, High-accuracy inertial measurements with cold-atom sensors, AVS Quantum Science **2**, 024702 (2020).

[17] B. Canuel, A. Bertoldi, L. Amand, E. Pozzo di Borgo, T. Chantrait, C. Danquigny, M. Dovale Alvarez, B. Fang, A. Freise, R. Geiger *et al.*, Exploring gravity with the miga large scale atom interferometer, Sci. Rep. **8**, 14064 (2018).

[18] C Jekeli, Navigation error analysis of atom interferometer inertial sensor, Navigation **52**, 1 (2005).

[19] B. Battelier, B. Barrett, L. Fouche, L. Chichet, L. Antoni-Micollier, H. Porte, F. Napolitano, J. Lautier, A. Landragin, and P. Bouyer, Development of compact cold-atom sensors for inertial navigation, in *Quantum Optics*, edited by J. Stuhler and A. J. Shields, International Society for Optics and Photonics (SPIE, Bellingham, WA, 2016), Vol. 9900, p. 990004

[20] P. Cheiney, L. Fouche, S. Templier, F. Napolitano, B. Battelier, P. Bouyer, and B. Barrett, Navigation-compatible hybrid quantum accelerometer using a Kalman filter, Phys. Rev. Appl. **10**, 034030 (2018).

[21] S. Dimopoulos, P. W. Graham, J. M. Hogan, and M. A. Kasevich, Testing general relativity with atom interferometry, Phys. Rev. Lett. **98**, 111102 (2007).

[22] S. A Haine, Searching for signatures of quantum gravity in quantum gases, New J. Phys. **23**, 033020 (2021).

[23] G. M. Tino, Testing gravity with cold atom interferometry: results and prospects, Quantum Sci. Technol. **6**, 024014 (2021).

[24] L. Pezze, A. Smerzi, M. K. Oberthaler, R. Schmied, and P. Treutlein, Quantum metrology with nonclassical states of atomic ensembles, Rev. Mod. Phys. **90**, 035005 (2018).

[25] S. S. Szigeti, O. Hosten, and S. A. Haine, Improving cold-atom sensors with quantum entanglement: Prospects and challenges, Appl. Phys. Lett. **118**, 140501 (2021).

[26] S. Colombo, E. Pedrozo-Penafiel, and V. Vuletic, Entanglement-enhanced optical atomic clocks, Appl. Phys. Lett. **121**, 210502 (2022).

[27] M. Kitagawa and M. Ueda, Squeezed spin states, Phys. Rev. A **47**, 5138 (1993).

[28] J. Esteve, C. Gross, A. Weller, S. Giovanazzi, and M. K. Oberthaler, Squeezing and entanglement in a Bose-Einstein condensate, Nature (London) **455**, 1216 (2008).

[29] C. Gross, T. Zibold, E. Nicklas, J. Esteve, and M. K. Oberthaler, Nonlinear atom interferometer surpasses classical precision limit, Nature (London) **464**, 1165 (2010).

[30] M. F. Riedel, P. Böhi, Y. Li, T. W. Hänsch, A. Sinatra, and P. Treutlein, Atom-chip-based generation of entanglement for quantum metrology, Nature (London) **464**, 1170 (2010).

[31] J. Appel, P. J. Windpassinger, D. Oblak, U. B. Hoff, N. Kjaergaard, and E. S. Polzik, Mesoscopic atomic entanglement for precision measurements beyond the standard quantum limit, Proc. Natl. Acad. Sci. USA **106**, 10960 (2009).

[32] T. Takano, M. Fuyama, R. Namiki, and Y. Takahashi, Spin squeezing of a cold atomic ensemble with the nuclear spin of one-half, Phys. Rev. Lett. **102**, 033601 (2009).

[33] A. Louchet-Chauvet, J. Appel, J. J. Renema, D. Oblak, N. Kjaergaard, and E. S. Polzik, Entanglement-assisted atomic clock beyond the projection noise limit, New J. Phys. **12**, 065032 (2010).

[34] M. Koschorreck, M. Napolitano, B. Dubost, and M. W. Mitchell, Quantum nondemolition measurement of large-spin ensembles by dynamical decoupling, Phys. Rev. Lett. **105**, 093602 (2010).

[35] M. H. Schleier-Smith, I. D. Leroux, and V. Vuletic, Squeezing the collective spin of a dilute atomic ensemble by cavity feedback, Phys. Rev. A **81**, 021804(R) (2010).

[36] I. D. Leroux, M. H. Schleier-Smith, and V. Vuletic, Implementation of cavity squeezing of a collective atomic spin, Phys. Rev. Lett. **104**, 073602 (2010).

[37] R. J. Sewell, M. Koschorreck, M. Napolitano, B. Dubost, N. Behbood, and M. W. Mitchell, Magnetic sensitivity beyond the projection noise limit by spin squeezing, Phys. Rev. Lett. **109**, 253605 (2012).

[38] O. Hosten, N. J. Engelsen, R. Krishnakumar, and M. A. Kasevich, Measurement noise 100 times lower than the quantum-projection limit using entangled atoms, Nature (London) **529**, 505 (2016).

[39] G. P. Greve, C. Luo, B. Wu, and J. K. Thompson, Entanglement-enhanced matter-wave interferometry in a high-finesse cavity, Nature (London) **610**, 472 (2022).

[40] M. Kritsotakis, J. A. Dunningham, and S. A. Haine, Spin squeezing of a Bose-Einstein condensate via a quantum nondemolition measurement for quantum-enhanced atom interferometry, Phys. Rev. A **103**, 023318 (2021).

[41] S. S. Szigeti, S. P. Nolan, J. D. Close, and S. A. Haine, High-precision quantum-enhanced gravimetry with a Bose-Einstein condensate, Phys. Rev. Lett. **125**, 100402 (2020).

[42] D. J. Wineland, J. J. Bollinger, W. M. Itano, F. L. Moore, and D. J. Heinzen, Spin squeezing and reduced quantum noise in spectroscopy, Phys. Rev. A **46**, R6797 (1992).

[43] A. Kuzmich, N. P. Bigelow, and L. Mandel, Atomic quantum non-demolition measurements and squeezing, Europhys. Lett. **42**, 481 (1998).

[44] D. Oblak, P. G. Petrov, C. L. Garrido Alzar, W. Tittel, A. K. Vershovski, J. K. Mikkelsen, J. L. Sørensen, and E. S. Polzik, Quantum-noise-limited interferometric measurement of atomic noise: Towards spin squeezing on the Cs clock transition, Phys. Rev. A **71**, 043807 (2005).

[45] M. Saffman, D. Oblak, J. Appel, and E. S. Polzik, Spin squeezing of atomic ensembles by multicolor quantum nondemolition measurements, Phys. Rev. A **79**, 023831 (2009).

[46] P. J. Windpassinger, D. Oblak, U. B. Hoff, J. Appel, N. Kjaergaard, and E. S. Polzik, Inhomogeneous light shift effects on atomic quantum state evolution in non-destructive measurements, New J. Phys. **10**, 053032 (2008).

[47] S. R. de Echaniz, M. W. Mitchell, M. Kubasik, M. Koschorreck, H. Crepaz, J. Eschner, and E. S. Polzik, Conditions for spin squeezing in a cold ^{87}Rb ensemble, J. Opt. B: Quantum Semiclassical Opt. **7**, S548 (2005).

[48] K. Hammerer, K. Mølmer, E. S. Polzik, and J. I. Cirac, Light-matter quantum interface, Phys. Rev. A **70**, 044304 (2004).

[49] A. Sørensen, L. M. Duan, J. I. Cirac, and P. Zoller, Many-particle entanglement with Bose–Einstein condensates, Nature (London) **409**, 63 (2001).

[50] Y. Li, Y. Castin, and A. Sinatra, Optimum spin squeezing in Bose-Einstein condensates with particle losses, Phys. Rev. Lett. **100**, 210401 (2008).

[51] Y. Li, P. Treutlein, J. Reichel, and A. Sinatra, Spin squeezing in a bimodal condensate: spatial dynamics and particle losses, Eur. Phys. J. B **68**, 365 (2009).

[52] S. A. Haine and M. T. Johnsson, Dynamic scheme for generating number squeezing in Bose-Einstein condensates through nonlinear interactions, Phys. Rev. A **80**, 023611 (2009).

[53] S. A. Haine, J. Lau, R. P. Anderson, and M. T. Johnsson, Self-induced spatial dynamics to enhance spin squeezing via one-axis twisting in a two-component Bose-Einstein condensate, Phys. Rev. A **90**, 023613 (2014).

[54] T. Laudat, V. Dugrain, T. Mazzoni, M.-Z. Huang, C. L. G. Alzar, A. Sinatra, P. Rosenbusch, and J. Reichel, Spontaneous spin squeezing in a Rubidium BEC, New J. Phys. **20**, 073018 (2018).

[55] R. Corgier, N. Gaaloul, A. Smerzi, and L. Pezzè, Delta-kick squeezing, Phys. Rev. Lett. **127**, 183401 (2021).

[56] D. F. Walls and G. J. Milburn, *Quantum Optics*, 2nd ed. (Springer-Verlag, Berlin, 2008).

[57] M. J. Steel, M. K. Olsen, L. I. Plimak, P. D. Drummond, S. M. Tan, M. J. Collett, D. F. Walls, and R. Graham, Dynamical quantum noise in trapped Bose-Einstein condensates, Phys. Rev. A **58**, 4824 (1998).

[58] A. Sinatra, C. Lobo, and Y. Castin, The truncated Wigner method for Bose-condensed gases: limits of validity and applications, J. Phys. B: At., Mol. Opt. Phys. **35**, 3599 (2002).

[59] A. A. Norrie, R. J. Ballagh, and C. W. Gardiner, Quantum turbulence and correlations in Bose-Einstein condensate collisions, Phys. Rev. A **73**, 043617 (2006).

[60] P. D. Drummond and B. Opanchuk, Truncated Wigner dynamics and conservation laws, Phys. Rev. A **96**, 043616 (2017).

[61] S. A. Haine and A. J. Ferris, Surpassing the standard quantum limit in an atom interferometer with four-mode entanglement produced from four-wave mixing, Phys. Rev. A **84**, 043624 (2011).

[62] B. Opanchuk, M. Egorov, S. Hoffmann, A. I. Sidorov, and P. D. Drummond, Quantum noise in three-dimensional BEC interferometry, Europhys. Lett. **97**, 50003 (2012).

[63] J. Ruostekoski and A. D. Martin, The Truncated Wigner method for Bose gases, in *Quantum Gasses*, edited by T. Editor (Imperial College Press, London, 2013), pp. 203–214.

[64] S. P. Nolan, J. Sabbatini, M. W. J. Bromley, M. J. Davis, and S. A. Haine, Quantum enhanced measurement of rotations with a spin-1 Bose-Einstein condensate in a ring trap, Phys. Rev. A **93**, 023616 (2016).

[65] S. A Haine, Quantum noise in bright soliton matterwave interferometry, New J. Phys. **20**, 033009 (2018).

[66] S. A. Haine and W. Y. S. Lau, Generation of atom-light entanglement in an optical cavity for quantum enhanced atom interferometry, Phys. Rev. A **93**, 023607 (2016).

[67] P. D. Drummond and A. D. Hardman, Simulation of quantum effects in Raman-active waveguides, Europhys. Lett. **21**, 279 (1993).

[68] P. B. Blakie, A. S. Bradley, M. J. Davis, R. J. Ballagh, and C. W. Gardiner, Dynamics and statistical mechanics of ultra-cold Bose gases using c-field techniques, Advances in Physics, Adv. Phys. **57**, 363 (2008).

[69] C. W. Gardiner and P. Zoller, *Quantum Noise: A Handbook of Markovian and Non-Markovian Quantum Stochastic Methods with Applications to Quantum Optics*, 3rd ed. (Springer, Berlin, 2004).

[70] M. K. Olsen and A. S. Bradley, Numerical representation of quantum states in the positive-P and Wigner representations, Opt. Commun. **282**, 3924 (2009).

[71] E. Pedrozo-Peñafiel, S. Colombo, C. Shu, A. F. Adiyatullin, Z. Li, E. Mendez, B. Braverman, A. Kawasaki, D. Akamatsu, Y. Xiao, and V. Vuletić, Entanglement on an optical atomic-clock transition, Nature **588**, 414 (2020).

[72] Z. Li, B. Braverman, S. Colombo, C. Shu, A. Kawasaki, A. F. Adiyatullin, E. Pedrozo-Peñafiel, E. Mendez, and V. Vuletić, Collective spin-light and light-mediated spin-spin interactions in an optical cavity, PRX Quantum **3**, 020308 (2022).

[73] S. A. Haine, Using interaction-based readouts to approach the ultimate limit of detection-noise robustness for quantum-enhanced metrology in collective spin systems, Phys. Rev. A **98**, 030303(R) (2018).

[74] O. Hosten, R. Krishnakumar, N. J. Engelsen, and M. A. Kasevich, Quantum phase magnification, Science **352**, 1552 (2016).

[75] D. Barberena, D. Chu, J. K. Thompson, and A. M. Rey, Trade-offs between unitary and measurement induced spin squeezing in cavity QED, arXiv:2309.15353 (2023).